Online System Identification of the dynamics of an Autonomous Underwater Vehicle

Eng You Hong
ARL, Tropical Marine Science Institute,
National University of Singapore,
Singapore.
tmseyh@nus.edu.sg

Teo Kwong Meng
Dept. of Industrial & System Engineering,
National University of Singapore,
Singapore.
kwongmeng@nus.edu.sg

Mandar Chitre
ARL, Tropical Marine Science Institute,
National University of Singapore,
Singapore.
mandar@nus.edu.sg

***Abstract*—Autonomous Underwater vehicles (AUV) with reconfigurable payloads are rapidly becoming common. Their dynamic characteristics are affected when payloads change. Typically, retuning of the controller is required to maintain good control performance. To address this situation, we develop a technique to enable rapid identification of AUV dynamics online. We demonstrate the technique with a fin-controlled single-thruster torpedo-shaped AUV. By decoupling the system according to planar and horizontal motion, mathematical models for yaw and pitch dynamics are developed. This results in a second-order transfer function with auxiliary steady state fin deflection. Identification of continuous-time model was performed to preserve the physical meaning of the parameters. Identification in continuous-time requires time-derivative terms which are reconstructed using the state variable filter (SVF). Then, recursive least-square (RLS) algorithm is used to identify the unknown parameters. The proposed identification method was validated through field deployments of our AUVs. The online estimates compare favorably with results obtained from offline identification methods requiring numerical optimization. We demonstrate how turning radius of the AUV can be estimated accurately from the identified parameters. We also show how a gain-scheduled controller, with better control performance than a constant-gain controller, can be designed using the estimated parameters.**

I. Introduction

Most autonomous underwater vehicle (AUV) controllers are model-based. So their performance strongly depends on the accuracy of the model parameters. Traditionally, those parameters are obtained through tow-tank experiments using a planar motion mechanism (PMM) or by employing computational fluid dynamics (CFD) analysis. Both methods are time consuming and expensive to carry out. We frequently work with modular AUVs where the payload configuration changes frequently. It is operationally infeasible to employ those two methods each time there is a change in the payload configuration.

As an alternative, one can perform on-board sensor system identification to obtain parameters of a simplified model. An initial controller is designed based on a rough estimate of the parameters. The goal is to control the AUV to the operating condition where open loop testing can be carried out. Based on the input-output data, model parameters are found by matching the simulated model output with the true vehicle response. The test only makes use of the on-board sensors to measure the vehicle response under known input excitation. With that, a dynamic model can be identified rapidly from AUV flight data and a revised controller can be redesigned on-the-fly.

Most of the identification methods reported for unmanned underwater vehicles (UUVs) are offline operated and mostly applied to the open-frame vehicles [1], [2]. An online adaptive identification technique had been proposed by Smallwood and Whitcomb [3] for application in their JHUROV remotely operated underwater vehicle (ROV). Ridao *et al.* [2] compared two identification methods using URIS UUV; one is based on the minimization of the acceleration prediction error and another is based on the minimization of the velocity one-step prediction error. For application to streamlined AUVs, work had been done by Rentschler *et al.* [4] where system identification was performed offline using an optimization technique. Tiano *et al.* [5] proposed an observer Kalman filter identification method which can be run online. Both simulation and experimental result were presented, but restricted to yaw dynamics of the Hammerhead AUV. Discrete-time model was used instead of a continuous-time model. Recently, Petrich *et al.* [6] studied offline identification of the pitch axis of Virginia Tech 475 AUV. They argued that the linear second order pitch model suffices for the purpose of attitude control design. The online implementation of their algorithm was not discussed.

We demonstrate a technique for online system identification on the STARFISH AUV [7] based on state variable filter (SVF) and recursive least-square (RLS) estimator. While the SVF-RLS approach to identification for continuous-time model is well known [8], the application to AUV and the experimental evaluation reported here is new. The proposed method is simpler to implement and requires selection of fewer design parameters as compared to existing methods using adaptive identifier [3] and nonlinear observer [9]. In section II, we decouple the AUV dynamics according to planar and horizontal motion. The respective mathematical models for yaw and pitch dynamics are developed. The identification problem is formulated in section III. Two methods to identify the unknown parameters are discussed. The first method is based on an offline nonlinear optimization via simulation, which we use as a benchmark for our proposed online method. The online method utilizes a SVF filter to reconstruct the time-derivative from sampled data and a RLS estimator to find the unknown parameters. We validated this identification method through

field deployments of our AUV. The details of experimental design and results are discussed in section IV. In section V, we make use of yaw identification results to estimate the turning radius of the AUV at different speeds. In section VI, we show how a gain-scheduled controller can be designed using the identified parameters. Lastly, some concluding remarks are presented in section VII.

II. Modeling of Yaw and Pitch Dynamics of AUV

Generally, the motion of an AUV can be described using six degrees of freedom differential equations of motion [10]. These equations are developed using two coordinate frames shown in Fig. 1. Six velocity components $[u, v, w, p, q, r]$ (surge, sway, heave, roll, pitch, yaw) are defined in the body-fixed frame, while the earth-fixed frame defines the corresponding positions and attitudes $[x, y, z, \phi, \theta, \psi]$. The notation used in this paper is in accordance with SNAME [11].

When designing a controller for the AUV, we follow the conventional control philosophy which divides the AUV into three subsystems [12]. They are: (1) steering subsystem to control the heading by using rudder, (2) diving subsystem to control depth and pitch by using the elevator, and (3) speed subsystem to control vehicle speed by varying the propeller speed. The divide-and-conquer methodology works well in practice for streamlined AUVs when the coupling between subsystems is weak. In this section, we developed the yaw and pitch dynamics of the AUV. A nonlinear model is derived from first principles. By making some decoupling assumptions, we then propose an approximate linear model for use in yaw and pitch identification respectively.

A. Yaw Dynamics

By making the following assumptions, we restrict the motion of the AUV in the steering plane (x-y plane):

1) heave velocity $w = 0$.
2) roll $\phi = 0$.
3) constant pitch $\theta = \theta_o \Rightarrow$ pitch rate $\dot{\theta} = 0$.

The equations of motion for sway and yaw are:

$$m(\dot{v} - u_0 r) = Y \tag{1}$$

$$I_z \dot{r} = N \tag{2}$$

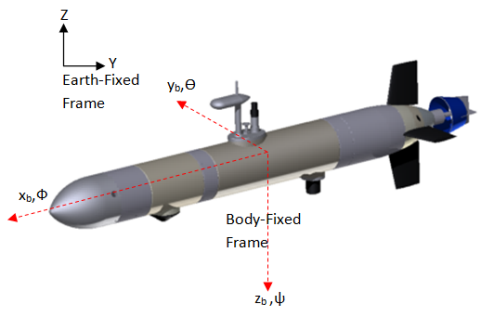

Fig. 1. Reference frame of STARFISH AUV.

The sway external force Y and yaw moments N consist of hydrodynamics added mass, linear damping, cross flow drag, munk moment and effect of rudder plane deflection.

$$Y = Y_{\dot{v}}\dot{v} + Y_{\dot{r}}\dot{r} + Y_v v + Y_r r + Y_\delta(\delta_r + \delta_{r_0}) \tag{3}$$

$$N = N_{\dot{v}}\dot{v} + N_{\dot{r}}\dot{r} + N_v v + N_r r + N_\delta(\delta_r + \delta_{r_0}) \tag{4}$$

For small roll and pitch angles, we have:

$$\dot{\psi} = \frac{sin\theta}{cos\theta} q + \frac{cos\phi}{cos\theta} r \approx r \tag{5}$$

Substituting (3) and (4) into (1) and (2) respectively and combining with (5), we can write the following state space representation using state variable $v(t)$, $r(t)$, $\psi(t)$:

$$\begin{bmatrix} \dot{v} \\ \dot{r} \\ \dot{\psi} \end{bmatrix} = \begin{bmatrix} -a_{11} & -a_{12} & 0 \\ -a_{21} & -a_{22} & 0 \\ 0 & 1 & 0 \end{bmatrix} \begin{bmatrix} v \\ r \\ \psi \end{bmatrix} + \begin{bmatrix} b_1 \\ b_2 \\ 0 \end{bmatrix} (\delta_r + \delta_{r_0}) \tag{6}$$

From experience, the sway velocity v during operation is small. Thus, the yaw dynamics are:

$$\dot{\psi} = r \tag{7}$$

$$\dot{r} = -a_{22} r + b_2(\delta_r + \delta_{r_0}) \tag{8}$$

The above derivation of the steering subsystem model follows the derivation in [12] closely but takes into the consideration of the steady state rudder deflection δ_{r_0}. The non-zero steady state rudder deflection is mainly caused by offset exist in the zero position of the rudder.

Rewriting (8), we have three parameters to be identified:

$$\dot{r} = \begin{bmatrix} -r & \delta_r & 1 \end{bmatrix} \begin{bmatrix} a_{22} \\ b_2 \\ C_0 \end{bmatrix} \tag{9}$$

where $C_0 = b_2\delta_{r_0}$. Applying a Laplace Transform and a change of variable to (8), we have:

$$\frac{\psi(S)}{\delta_r'(S)} = \frac{b_2}{s^2 + a_{22}s}, \delta_r'(S) = \mathcal{L}(\delta_r + \delta_{r_0}) \tag{10}$$

B. Pitch Dynamics

By making the following assumptions, we restrict the motion of the AUV in the diving plane (x-z plane):

1) sway velocity $v = 0$.
2) roll $\phi = 0$.
3) constant heading $\psi = \psi_o \Rightarrow$ yaw rate $\dot{\psi} = 0$.

The equations of motion for heave and pitch are:

$$m(\dot{w} - u_0 q) = Z \tag{11}$$

$$I_y \dot{q} = M \tag{12}$$

The heave external force Z and pitch moments M consist of hydrodynamics added mass, linear damping, cross flow drag, Munk moment and effect of elevator plane deflection. In addition, there is righting moment in pitch due to the vertical distance between center of mass and center of buoyancy $BG_z = z_G - z_B$. There is also excessive positive buoyancy of the vehicle $\Delta B = B - mg$ that acts in z-axis.

$$Z = Z_{\dot{w}}\dot{w} + Z_{\dot{q}}\dot{q} + Z_w w + Z_q q + Z_\delta \delta_s + \Delta B \tag{13}$$

$$
\begin{aligned}
M &= M_{\dot{w}}\dot{w} + M_{\dot{q}}\dot{q} + M_w w + M_q q \\
&\quad -mg(z_G - z_B)\sin\theta + M_\delta \delta_s \\
&\simeq M_{\dot{w}}\dot{w} + M_{\dot{q}}\dot{q} + M_w w + M_q q \\
&\quad -mgBG_z\theta + M_\delta \delta_s \qquad (14)
\end{aligned}
$$

From kinematics analysis in x-z plane with assumption of small pitch angle, we have:

$$\dot{\theta} = q \qquad (15)$$

$$\dot{z} = -\theta u_0 + w \qquad (16)$$

Substituting (13) and (14) into (11) and (12) respectively and combining with (15) and (16), we can write the following state space representation using state variable $w(t)$, $q(t)$, $\theta(t)$, and $z(t)$:

$$
\begin{aligned}
\begin{bmatrix} \dot{w} \\ \dot{q} \\ \dot{\theta} \\ \dot{z} \end{bmatrix} &= \begin{bmatrix} -c_{11} & -c_{12} & -c_{13} & 0 \\ -c_{21} & -c_{22} & -c_{23} & 0 \\ 0 & 1 & 0 & 0 \\ 1 & 0 & -u_0 & 0 \end{bmatrix} \begin{bmatrix} w \\ q \\ \theta \\ z \end{bmatrix} \\
&\quad + \begin{bmatrix} d_1 \\ d_2 \\ 0 \\ 0 \end{bmatrix} \delta_s + \begin{bmatrix} e_1 \\ e_2 \\ 0 \\ 0 \end{bmatrix} \Delta B \qquad (17)
\end{aligned}
$$

By assuming the value of $c_{21}w$ to be constant as heave velocity does not fluctuate significantly during a run, the linear model in (17) reduces to:

$$
\begin{aligned}
\begin{bmatrix} \dot{q} \\ \dot{\theta} \\ \dot{z} \end{bmatrix} &= \begin{bmatrix} -c_{22} & -c_{23} & 0 \\ 1 & 0 & 0 \\ 0 & -u_0 & 0 \end{bmatrix} \begin{bmatrix} q \\ \theta \\ z \end{bmatrix} \\
&\quad + \begin{bmatrix} d_2 \\ 0 \\ 0 \end{bmatrix} \delta_s + \begin{bmatrix} c_{21}w + e_2\Delta B \\ 0 \\ 0 \end{bmatrix} \qquad (18)
\end{aligned}
$$

Thus, the pitch dynamics are:

$$\dot{\theta} = q \qquad (19)$$

$$\dot{q} = -c_{22}q - c_{23}\theta + d_2\delta_s + C_b \qquad (20)$$

where

$$C_b = c_{21}w + e_2\Delta B \qquad (21)$$

The above derivation of the depth subsystem model follows the derivation in [12] closely but takes into the consideration that the AUV is positive buoyant. From experimental measurements, the resulting heave velocity is around 0.13 m/s and therefore it is not negligible. In [12], the heave velocity is small (less than 0.05 m/s). The heave velocity introduces cross flow drag and Munk moment which result in an offset term C_b that needs to be compensated by the pitch controller.

Rewriting (20), we have four parameters to be identified:

$$\dot{q} = \begin{bmatrix} -q & -\theta & \delta & 1 \end{bmatrix} \begin{bmatrix} c_{22} \\ c_{23} \\ d_2 \\ C_b \end{bmatrix} \qquad (22)$$

Equation (20) can also be rewritten in the following form by introduce a new term, steady state elevator deflection δ_{s_0}:

$$
\begin{aligned}
\dot{q} &= -c_{22}q - c_{23}\theta + d_2(\delta_s + \frac{C_b}{d_2}) \qquad (23) \\
\dot{q} + c_{22}q + c_{23}\theta &= d_2(\delta_s + \delta_{s_0})
\end{aligned}
$$

Applying Laplace Transform and a change of variable, we have:

$$\frac{\theta(S)}{\delta'_s(S)} = \frac{d_2}{s^2 + c_{22}s + c_{23}}, \delta'_s(S) = \mathcal{L}(\delta_s + \delta_{s_0}) \qquad (24)$$

III. Identification Method

A. Problem Formulation

Equations (9) and (20) can be written in the following forms:

$$
\begin{aligned}
\frac{d^2\psi}{dt^2} + a_{22}\frac{d\psi}{dt} &= b_2\delta_r + C_o \\
\frac{d^2\theta}{dt^2} + c_{22}\frac{d\theta}{dt} + c_{23}\theta &= d_2\delta_s + C_b
\end{aligned} \qquad (25)
$$

These equations fall into the following generalized framework. Consider a single-input, single-output, linear, time-invariant, continuous-time system having noise-free input $u_0(t)$ and output $y_0(t)$ linked by:

$$
\begin{aligned}
&y^{(n)}(t) + \alpha_1 y^{(n-1)}(t) + \ldots + \alpha_n y(t) \\
&= \beta_0 u^{(m)}(t) + \beta_1 u^{(m-1)}(t) + \ldots + \beta_m u(t) + C
\end{aligned} \qquad (26)
$$

where $x^{(j)}(t) = \frac{d^j x(t)}{dt^j}$.

The system is assumed to be proper, i.e., $m \leq n$. Without any loss of generality we assume $\alpha_0 = 1$. It is assumed that the input and output signals are sampled at time instants $\{t_k\}_{k=1}^N$. The sampled signals are denoted by $\{u_0(t_k); y_0(t_k)\}$.

The identification problem consists of using input/output discrete data $\{u_0(t_k); y_0(t_k)\}$, $k = 1....N$, to determine the values of parameters $\{\alpha_j\}_{j=1}^n$ and $\{\beta_j\}_{j=1}^m$ while satisfying certain goodness-of-fit constraints between predicted data and measurement. Here, N is the total number of samples available. This can be expressed as:

$$
\begin{aligned}
\underset{\{\alpha_j\}_{j=1}^n, \{\beta_j\}_{j=1}^m}{\arg\min} \quad & J(\Theta) = \sqrt{\frac{1}{N}\sum_{i=1}^{i=N}[y^{(n)}(t_i) - \Phi(t_i)\Theta]^2} \\
\text{subject to} \quad & \{\alpha_j\}_{j=1}^n, \{\beta_j\}_{j=1}^m \in \Re
\end{aligned} \qquad (27)
$$

where

$$
\begin{aligned}
\Phi(t_i) = [\ & -y^{(n-1)}(t_i) \quad \ldots \quad -y(t_i) \\
& u^{(m)}(t_i) \quad \ldots \quad u(t_i) \quad 1]^T
\end{aligned} \qquad (28)
$$

and

$$\Theta = \begin{bmatrix} \alpha_1 & \ldots & \alpha_n & \beta_0 & \ldots & \beta_m & C \end{bmatrix}^T \qquad (29)$$

In the following sections, we discuss two methods to identify the unknown parameters Θ. The two methods are:

- Method 1: Nonlinear optimization via simulation.
- Method 2: SVF and RLS with forgetting factor.

B. Nonlinear Optimization via Simulation

The simulation process takes time-stamped field data input (rudder or elevator deflection) along with the AUV initial state (positions and rates) and then proceeds to simulate the vehicle's response using (25). Given initial input parameters and field measurements, the optimization process searches iteratively for a solution that minimizes the difference in the yaw/pitch of the field data with the simulated yaw/pitch response.

The algorithm does not require time-derivative of the yaw/pitch. However, it is important to note that a numerical minimization can only be applied after the entire data set is collected. Hence, the ability to perform system identification via simulation is limited to offline parameter estimation. If the solution space is convex, the numerical optimization method will give optimal solution that minimize the cost function $J(\Theta)$ for that particular set of data. We will use this offline method as a benchmark for our online methods discussed next.

C. SVF and RLS with forgetting factor

1) SVF: Reconstructing time-derivative from sampled data is an important step in direct continuous-time model identification. Numerical computation of derivative via finite difference method is very sensitive to measurement noise. The traditional SVF approach overcomes this issue by passing both input/output signals through an all-pole filter $F(s)$ of minimum order n. It is preferable to choose $F(s)$ such that it has n similar poles [13]:

$$F(s) = \frac{1}{(s+\lambda)^n} \tag{30}$$

Let

$$\mathbf{y_f}(t) = \begin{bmatrix} y_f^{(n)}(t) & \dots & y_f^{(0)}(t) \end{bmatrix}^T \tag{31}$$

and

$$\mathbf{u_f}(t) = \begin{bmatrix} u_f^{(m)}(t) & \dots & u_f^{(0)}(t) \end{bmatrix}^T \tag{32}$$

Let us denote the Laplace transform of $y(t)$ and $u(t)$ as

$$\mathbf{Y}(s) = \mathcal{L}\{y(t)\} \tag{33}$$
$$\mathbf{U}(s) = \mathcal{L}\{u(t)\} \tag{34}$$

Then:

$$\begin{aligned} \mathbf{Y_f}(s) &= \mathcal{L}\{\mathbf{y_f}(t)\} \\ &= \frac{1}{(s+\lambda)^n} \begin{bmatrix} s^n & \dots & s & 1 \end{bmatrix}^T \mathbf{Y}(s) \end{aligned} \tag{35}$$

$$\begin{aligned} \mathbf{U_f}(s) &= \mathcal{L}\{\mathbf{u_f}(t)\} \\ &= \frac{1}{(s+\lambda)^m} \begin{bmatrix} s^m & \dots & s & 1 \end{bmatrix}^T \mathbf{U}(s) \end{aligned} \tag{36}$$

Note that the above filters are causally implementable. Here, we give an example on numerical implementation of the filter. The implementation is adopted from [13]. To obtain time-derivative of order two, we need following filter:

$$\mathbf{F(s)} = \begin{bmatrix} \frac{s^2}{(s+\lambda)^2} & \frac{s}{(s+\lambda)^2} & \frac{1}{(s+\lambda)^2} \end{bmatrix}^T \tag{37}$$

Let denote input signal to the filter as $w(t)$. The following state-space equations written in controllable canonical form can be used to obtained filter output:

$$\mathbf{y}(t) = \begin{bmatrix} w_f^{(2)} & w_f^{(1)} & w_f^{(0)} \end{bmatrix}^T \tag{38}$$
$$\mathbf{x}(t) = \begin{bmatrix} w_f^{(1)} & w_f^{(0)} \end{bmatrix}^T \tag{39}$$

$w_f^{(2)}$, $w_f^{(1)}$ and $w_f^{(0)}$ are the second, first and zero derivative of the filter input $w(t)$ respectively:

$$\dot{\mathbf{x}}(t) = \mathbf{A}\mathbf{x}(t) + \mathbf{B}w(t), \tag{40}$$
$$\mathbf{y}(t) = \mathbf{C}\mathbf{x}(t) + \mathbf{D}w(t), \tag{41}$$

with

$$\begin{aligned} \mathbf{A} &= \begin{bmatrix} -2\lambda & -1 \\ 1 & 0 \end{bmatrix}, \mathbf{B} = \begin{bmatrix} 1 \\ 0 \end{bmatrix}, \\ \mathbf{C} &= \begin{bmatrix} -2\lambda & -1 \\ 1 & 0 \\ 0 & 1 \end{bmatrix}, \mathbf{D} = \begin{bmatrix} 1 \\ 0 \\ 0 \end{bmatrix}. \end{aligned} \tag{42}$$

Under zero order hold (ZOH) assumption and with sampling interval, $h_k = t_{k+1} - t_k$, the above state space can be discretized into:

$$\dot{\mathbf{x}}(t_{k+1}) = \mathbf{A_d}\mathbf{x}(t_t) + \mathbf{B_d}w(t_k), \tag{43}$$
$$\mathbf{y}(t_k) = \mathbf{C_d}\mathbf{x}(t_k) + \mathbf{D_d}w(t_k), \tag{44}$$

with

$$\begin{aligned} &\mathbf{Ad} = e^{\mathbf{A}h_k}, \mathbf{Bd} = \left[e^{\mathbf{A}h_k} - \mathbf{I}\right]\mathbf{A}^{-1}, \\ &\mathbf{Cd} = \mathbf{C}, \mathbf{Dd} = \mathbf{D}. \end{aligned} \tag{45}$$

Fig. 2 illustrates a square pulse input u and its corresponding time-derivative for $\lambda = 2$. Filter constant λ is chosen to match the bandwidth of the system dynamics. In this study, we obtained consistent results for λ in the range of 2 to 8.

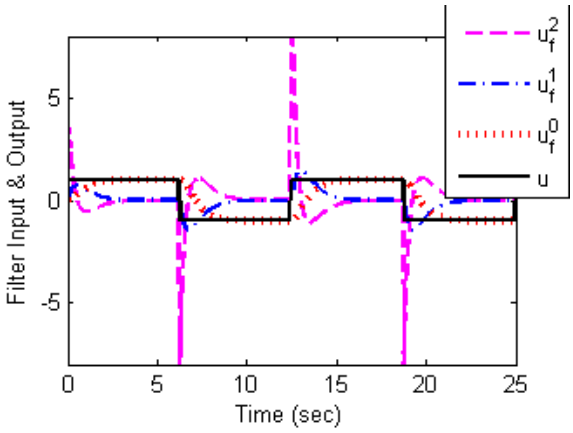

Fig. 2. Input and Output of the SVF filter for $\lambda = 2$

λ has to be chosen large enough such that the filtered signal contains useful information of the dynamics and small enough to filter out the measurement noise.

2) Block Least Square (BLS): Parameters in optimization problem (27) can be identified experimentally using standard least square method. Let N denote the total number of measurement available and define:

$$Q = \begin{bmatrix} y_f^{(n)}(t_1) & \dots & y_f^{(n)}(t_N) \end{bmatrix}^T \tag{46}$$

$$\mathbf{\Phi} = \begin{bmatrix} -y^{(n-1)}(t_1) & \dots & -y(t_1) & u^{(m)}(t_1) & \dots & u(t_1) & 1 \\ \vdots & & \vdots & \vdots & & & \\ -y^{(n-1)}(t_N) & \dots & -y(t_N) & u^{(m)}(t_N) & \dots & u(t_N) & 1 \end{bmatrix}$$

Thus if the $\mathbf{\Phi}$ is full rank, then the least square solution is given by the standard Moore-Penrose pseudoinverse:

$$\hat{\Theta} = (\mathbf{\Phi}^T\mathbf{\Phi})^{-1}\mathbf{\Phi}^T Q \tag{47}$$

3) RLS with forgetting factor: The idea behind RLS is to compute the parameters update $\hat{\Theta}(t)$ at each time instant t when measurement become available, by adding a correction term to the previous estimate $\hat{\Theta}(t-1)$. This saves a lot of computational effort as compared to the use of (47) with the entire measurement. It reduces the computational complexity from $O(N^3)$ to $O(N^2)$. For time-invariant system, the system parameters Θ are constant. However, for time-varying system, parameters change with time. In order to track the change in parameters, old data have to be forgotten and new data should have more weight in determining the parameters. The tracking capability of typical RLS can be improved by the *forgetting factor* technique. The idea is very simple; just add a forgetting factor β, where $0 < \beta \leq 1$, to give exponentially less weight to older samples.

A typical RLS algorithm with forgetting factor β has following form:

$$\hat{\Theta}(t) = \hat{\Theta}(t-1) + P(t)\Phi(t-1)\epsilon(t), \tag{48}$$

$$\epsilon(t) = y_f^{(n)}(t) - \Phi(t)\hat{\Theta}(t-1), \tag{49}$$

$$\tilde{P}(t) = P(t-1) - \frac{P(t-1)\Phi(t-1)\Phi(t-1)^T P(t-1)}{\beta + \Phi(t-1)^T P(t-1)\Phi(t-1)}, \tag{50}$$

$$P(t) = \frac{\tilde{P}(t)}{\beta}. \tag{51}$$

The algorithm requires an initial guess of $\Theta(t)$ and the covariance matrix P. The initial guess of $\Theta(t)$ is zero vector and P is $100\mathbf{I}_{n+m+1}$. $\mathbf{I}_{n+m+1}$ is the identity matrix of dimension $(n+m+1)$.

IV. Identification Results and Discussion

A. Experimental validation

The following experimental results are from data collected in Pandan Reservoir[1] using a STARFISH AUV called *GreenStar*. The GreenStar AUV carried a Thin Line Array (TLA) payload section in this experiment. The AUV was commanded to perform a straight run of 100 m at a depth of 2 m. When the AUV reached steady state (maintaining constant heading and depth), the excitation signal of ± 0.26 rad for 2 seconds respectively was injected into elevator deflection (Fig. 4d). The deflection generates moment in pitch axis and excites the pitch dynamics dramatically (Fig. 4b). After the excitation, the depth controller was switched on to return the AUV to the desired depth. The whole process was repeated for the second time for the richness of the data set. During the data collection, it is important to monitor the AUV's roll and yaw angle. Roll should be maintained near zero (Fig. 4a) and yaw angle should be maintained constant (Fig. 4c) in order to minimize the coupling effect. This is also illustrated in Fig. 3b where AUV was moving in a straight path in the x-y position plot.

The system identification can be performed based on the input $\delta(t)$ and output $\theta(t)$ to find out the value of c_{22}, c_{23}, d_2, C_b in (22). Table I reports the identified parameters obtained through methods 1 & 2. Method 1 was performed in Matlab using the Parameters Estimation Toolbox. The root mean square (RMS) error of pitch was found to be 0.025 rad. The table also reports parameters obtained via method 2. The RMS error of pitch was found to be 0.030 rad. Method 1 should produce minimal RMS error of pitch for this set of experimental data as it searches the entire parameters space. As the input/output data becomes available at each time instant, method 2 produces an estimate for the parameters as shown in Fig. 5. The parameters converge to their final value respectively from about 20 seconds onward. From Fig. 6, one can see a good agreement between the estimations produced by both methods and the measured data. We conclude that method 2 can be used to estimate parameters online as it produces estimates that accurately match the optimal parameters produced by method 1 offline.

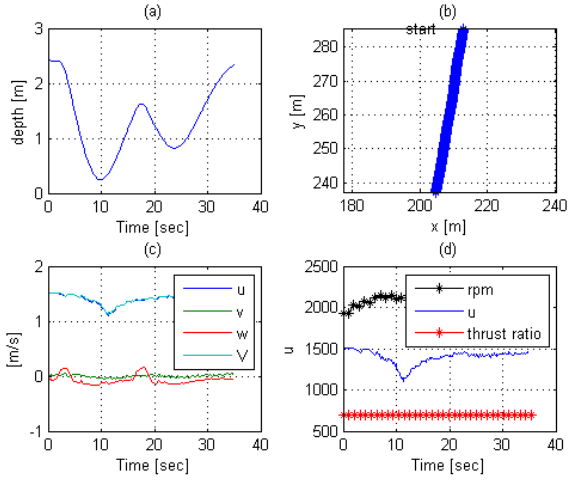

Fig. 3. Experiment run for identification for pitch dynamics at thrust ratio 70%. Plot of depth, x-y position, velocity and thrust ratio

[1]Pandan Reservoir is a reservoir located in the West Region of Singapore.

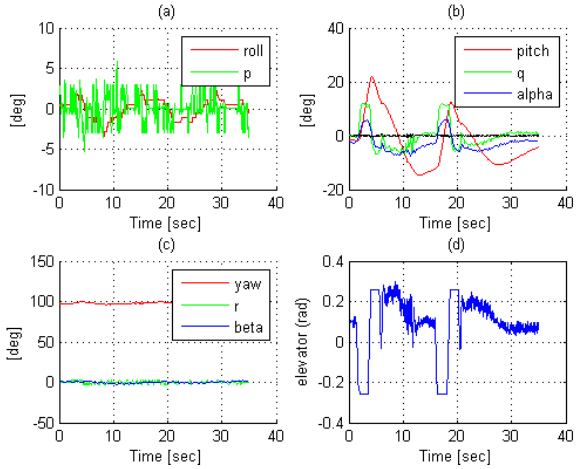

Fig. 4. Experiment run for identification for pitch dynamics at thrust ratio 70%. Plot of roll, pitch, yaw and elevator

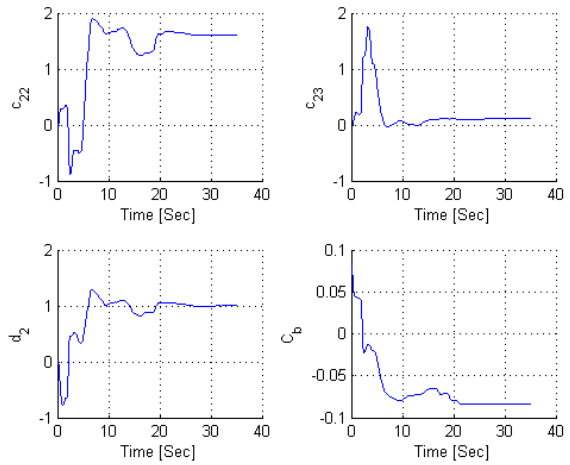

Fig. 5. Online parameters estimation of pitch dynamics at 70% thrust

B. Online system identification for yaw and pitch dynamics

The following experimental results are from data collected in Pandan Reservoir using STARFISH AUV called *RedStar*. The RedStar AUV carried a side-scan sonar payload in this experiment.

1) Identification for yaw dynamics: The AUV was commanded to perform a straight run of 100 m at a depth of 2 m. When the AUV reached steady state (maintaining constant heading and depth), the excitation signal of ± 0.26 rad for 2 seconds respectively was injected into rudder deflection (Fig. 8d). The deflection generates a moment around the yaw axis and excites the yaw dynamics dramatically (Fig. 8c). After the excitation, the yaw controller was switched on to return the AUV to the desired heading. The whole process was repeated for the second time for the richness of the data set. The rudder was set to ± 0.15 rad for the second excitation. During the identification process, the depth (Fig. 7a) and pitch (Fig. 8b) were kept approximately constant and roll was small (Fig. 8a).

TABLE I
PARAMETERS IDENTIFIED THROUGH OPTIMIZATION VIA SIMULATION (METHOD 1) AND SVF-RLS (METHOD 2)

	c_{22}	c_{23}	d_2	C_b	RMS Error (rad)
Optimization	1.56	0.09	0.99	-0.087	0.025
SVF-RLS	1.61	0.11	1.00	-0.084	0.030

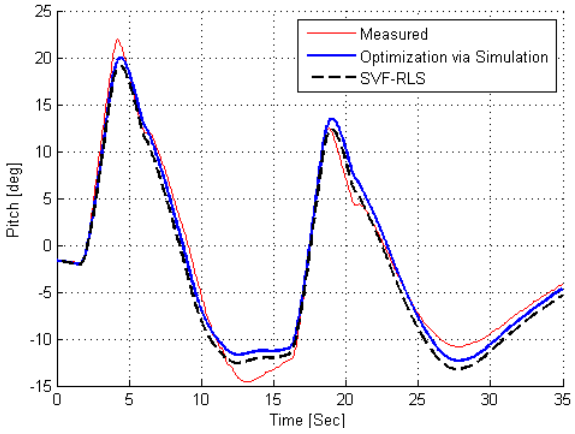

Fig. 6. Fitting of identified and measured pitch angle

Identification was enabled 2 seconds before the first excitation was given and ended 10 seconds after the second excitation was given. The whole process took 33 seconds in total, with 660 data points sampled at 20 Hz. The identification was only enabled during the resultant zig-zag maneuvering to fulfill the persistent excitation condition and have a better signal to noise ratio (SNR). Identification was repeated for different thrust values ranging from 60% to 100%. Parameters were set to zero initially. Fig. 9 shows how the parameter estimates evolve with time. Parameters a_{22} and b_2 converge after about 20 seconds. Parameters C_o stays close to zero with a consistent negative sign.

The results are summarized in Table II. The linear damping a_{22} has values around 1 with varying speeds. The negative value of a_{22} indicates that the yaw dynamics is inherently stable (poles are in the left-half plane). The rudder control authority b_2 increases with speed due to higher dynamic pressure at the control surfaces. Theoretically, the gain b_2 should vary linearly with the square of speed, u^2. This is verified in Fig. 10(a) which plot b_2 against u^2. The negative value of b_2 indicates that a positive rudder input creates a negative moment in yaw. The steady state rudder deflection δ_{r_0} reduces with increase in speed. This is due to the increase of control authority which requires smaller fin deflection to overcome the same yaw disturbance. The value of δ_{r_0} is almost zero. This indicates that there is no significant fin zero offset appearing at the rudder. This aligns with the fact that we calibrated the rudder position to eliminate the fin zero offset before the trial.

2) Identification for pitch dynamics: Identification for pitch dynamics was performed in the same way as described in section IV-A. The results are summarized in Table III and

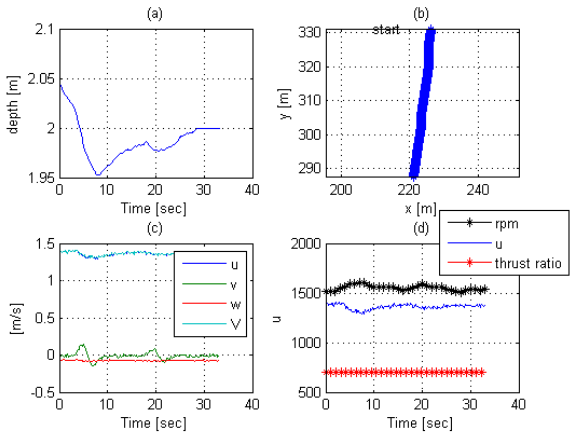

Fig. 7. Experiment run for identification for yaw dynamics at 70% thrust. Plot of depth, x-y position, velocity and thrust ratio

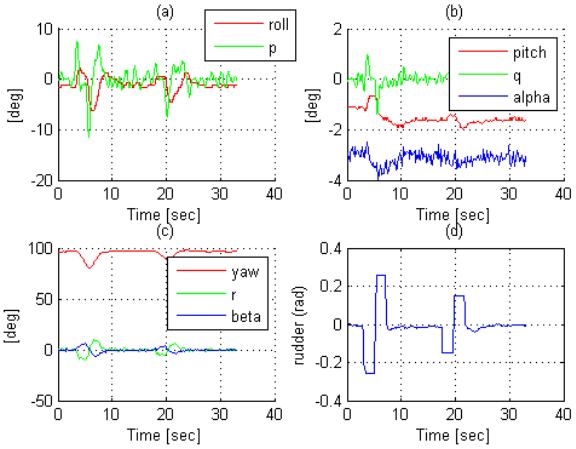

Fig. 8. Experiment run for identification for yaw dynamics at 70% thrust. Plot of roll, pitch, yaw and rudder

Fig. 11 shows how the parameters evolve with time. The linear damping term c_{22} and righting moment term c_{23} have values range between 2.1 to 2.6 and 0.02 to 0.05 respectively with varying speeds. The positive value of both c_{22} and c_{23} indicate that the pitch dynamics is inherently stable (poles are in the left-half plane) over the entire speed range. The elevator control authority d_2 increases with speed due to higher dynamics pressure at the control surfaces. Theoretically, the gain d_2 should vary linearly with the square in speed, u^2. This is verified in Fig. 10(b) which plot d_2 against u^2. The positive value of d_2 indicates that the positive rudder input creates positive moment in pitch. The magnitude of steady state elevator fin deflection δ_{s_0} reduces with increase of speed. In order to maintain constant depth, AUV needs to pitch down slightly to overcome its own buoyancy. The net buoyancy stays constant. However when AUV's thrust increases, the required pitch down angle θ_0 is reduced and thus the steady state elevator deflection.

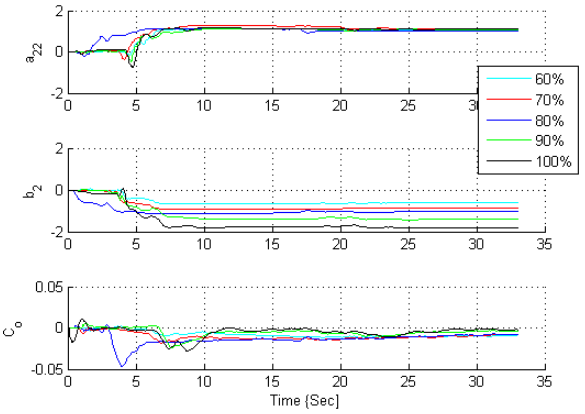

Fig. 9. Online parameters estimation of yaw dynamics for different thrusts

TABLE II
PARAMETERS IDENTIFIED FOR YAW DYNAMICS AT DIFFERENT THRUST RATIOS

Thrust (%)	Speed (m/s)	a_{22}	b_2	C_o	δ_{r_0}
60	1.07	1.04	-0.62	-0.0086	0.014
70	1.36	1.11	-0.86	-0.0082	0.010
80	1.63	1.01	-1.04	-0.0081	0.008
90	1.92	1.08	-1.41	-0.0042	0.003
100	2.19	1.10	-1.83	-0.0021	0.001

V. TURNING RADIUS OF AUV AT DIFFERENT SPEEDS

We would next like to make use of yaw identification results to estimate the turning radius of the AUV at different speeds. An understanding of the turning radius is especially important during maneuvering of the AUV for obstacle avoidance. It is also useful during path planning so that the achievable turning angle is taken into consideration.

We assume that the AUV has completed the yaw identification such that information present in Table II is available. For each speed, we require information of travel speed V, control authority b_2, and linear damping a_{22}. The rudder has a maximum deflection δ_{max} of 0.26 rad to avoid stalling. Fig. 12(a) illustrates an AUV making a U-turn with radius R. The perimeter of the half circle is πR. Let T_π denotes the time taken to make an 180 $\deg$ turn. Then, we have:

$$\pi R = V T_\pi \tag{52}$$

Fig. 12(b) shows a trapezoidal profile for yaw angular velocity. In order to make a U-turn, the AUV will start turning from zero yaw angular velocity to critical yaw angular velocity, $\dot{\psi}_{max}$. The acceleration process takes t_1 seconds. Then, it maintains turning rate at $\dot{\psi}_{max}$ for t_2 seconds before decelerating to zero. The deceleration process takes another t_1 seconds. So, we have:

$$T_\pi = t_1 + t_2 + t_1 \tag{53}$$

The area under the curve is the total heading change of π rad.

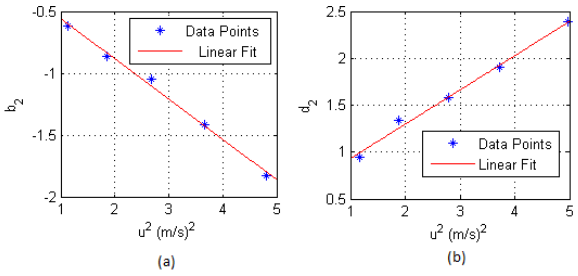

Fig. 10. (a) Plot of rudder control authority b_2 against speed^2 (b)Plot of elevator control authority d_2 against speed^2

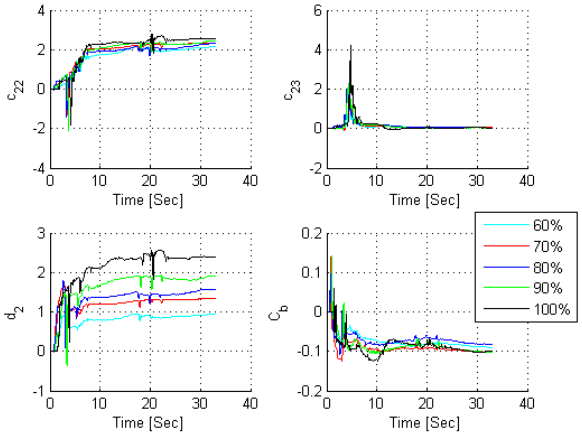

Fig. 11. Online parameters estimation of pitch dynamics for different thrusts

So,

$$\frac{1}{2}\dot{\psi}_{max}(t_2 + t_1 + t_2 + t_1) = \pi \tag{54}$$

$$\dot{\psi}_{max}(t_2 + t_1) = \pi \tag{55}$$

From (10), we know that the transfer function of yaw angular velocity to rudder is a first-order system:

$$\frac{\dot{\psi}(S)}{\delta_r(S)} = \frac{b_2}{s + a_{22}} \tag{56}$$

Under the step input of rudder at magnitude δ_{max}, the step response is

$$C(S) = \frac{b_2}{s + a_{22}} \cdot \frac{\delta_{max}}{s} \tag{57}$$

Taking the inverse transform, the step response is given by

$$c(t) = \frac{b_2\delta_{max}}{a_{22}}(1 - e^{-a_{22}t}) \tag{58}$$

By letting time go to infinity in (58), $\dot{\psi}_{max}$ is given by

$$\dot{\psi}_{max} = \frac{b_2\delta_{max}}{a_{22}} \tag{59}$$

The time t_1 is approximated by the time taken to reach 90% of the final value [14]:

$$t_1 = \frac{2.31}{a_{22}} \tag{60}$$

TABLE III
PARAMETERS IDENTIFIED FOR PITCH DYNAMICS AT DIFFERENT THRUST

Thrust (%)	Speed (m/s)	c_{22}	c_{23}	d_2	C_b	δ_{s_0} (rad)	θ_0 (deg)
60	1.09	2.13	0.052	0.94	-0.089	-0.095	-2.72
70	1.37	2.34	0.057	1.34	-0.100	-0.075	-1.53
80	1.67	2.31	0.031	1.58	-0.081	-0.051	-0.94
90	1.93	2.43	0.021	1.91	-0.102	-0.054	-0.40
100	2.23	2.57	0.033	2.39	-0.099	-0.042	-0.06

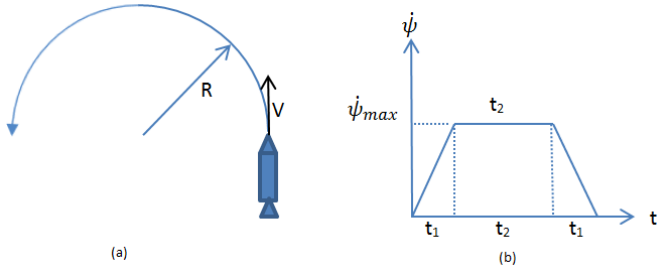

Fig. 12. (a) Turning Radius R of an AUV travel at speed, V and (b) Trapezoidal Profile for Yaw Angular velocity

Substituting (55), (59) and (60) into (53), we have:

$$T_\pi = \frac{\pi a_{22}}{b_2\delta_{max}} + \frac{2.31}{a_{22}} \tag{61}$$

and

$$R = V\left(\frac{a_{22}}{b_2\delta_{max}} + \frac{2.31}{a_{22}\pi}\right) \tag{62}$$

Table IV presents the results of turning radius at different speeds. The critical yaw angular velocity $\dot{\psi}_{max}$ increases with speed. From (59), $\dot{\psi}_{max}$ is linearly proportional to b_2, which in term is linearly proportional to the square of speed. As expected, the time taken to complete a U-turn T_π reduces with speed as the AUV turns at a faster rate. In general, the turning radius R reduces with speed but at a slower pace from 7.6 m to 6.5 m. The turning radius peaks at 70% thrust; smaller turning radius is possible at lower speeds.

In the following analysis, we predict turning radius at speeds that we did not perform identification at. From Table II, we assume a_{22} stays constant near 1. From Fig. 10, we have following relationship between speed V and b_2:

$$b_2 = 0.3263V^2 + 0.2319 \tag{63}$$

TABLE IV
TURNING RADIUS FOR AUV AT DIFFERENT SPEEDS

Thrust (%)	Speed V (m/s)	$\dot{\psi}_{max}$ (deg/s)	T_π (s)	R (m)
60	1.06	8.91	22.42	7.61
70	1.36	11.53	17.68	7.65
80	1.63	15.48	13.93	7.23
90	1.92	19.54	11.35	6.94
100	2.20	24.87	9.34	6.54

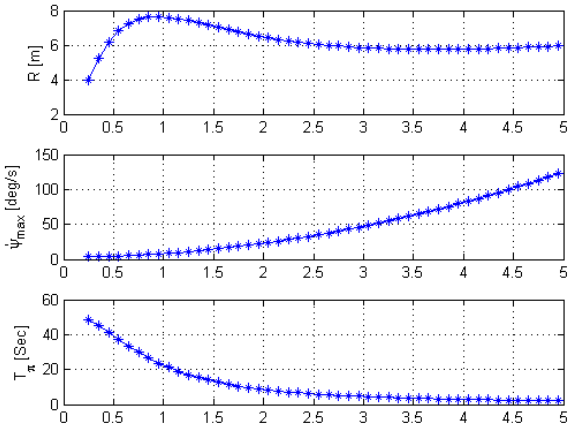

Fig. 13. Turning radius of AUV at different speeds

With $\delta_{max} = 0.26$ rad, we have:

$$R = V\left(\frac{1}{(0.3263V^2 + 0.2319)(0.26)} + \frac{2.31}{(1)\pi}\right) \tag{64}$$

Similarly, we have $\dot{\psi}_{max}$ and T_π as follow:

$$\dot{\psi}_{max} = 0.26(0.3263V^2 + 0.2319) \tag{65}$$

$$T_\pi = \frac{\pi}{0.26(0.3263V^2 + 0.2319)} + 2.31 \tag{66}$$

Fig. 13 predicts how turning radius R changes with speed. It is important to note that yaw identification was only performed for speed range from 1 to 2.2 m/s but the plot shows result for speeds from 0.5 to 5 m/s. The result is only valid if (63) and assumption $a_{22} = 1$ hold beyond the studied speed range.

The result shows that in order to achieve smaller turning radius, the AUV should travel at lower speeds. For example, at speed 0.25 m/s, the turning radius is 4 m. The trade off is it takes about 49 seconds to complete a U-turn. For the higher speed region, the minimum achievable turning radius is 5.75 m at speed of 3.7 m/s[2]. The turning radius increases with speed after that. There is a minimum value for T_π despite increase in speed. As $R \propto VT_\pi$, when V increases faster than the decrease in T_π, the turning radius will increase with speed.

A test was carried out to compare the measured turning radius against the predicted turning radius. A basic AUV with a Doppler Velocity Log (DVL) section was used in this experiment. The AUV was commanded to a constant depth of 2 m. It was asked to thrust at 70% with an average speed of 1.37 m/s. Yaw identification was executed to identified parameters a_{22}, b_2 and C_o. Then the AUV was commanded to make a U-turn before returning to the surface. The turning radius of the AUV was found by fitting a circle on the x-y position plot as illustrated in Fig. 14(a). Table V shows the identified parameters and the predicted $\dot{\psi}_{max}$, T_π and R. It is interesting to note that the δ_{r_0} is not equal to zero. In this case,

[2]The STARFISH AUV design top speed is only about 2.5 m/s, so this speed is not achievable in practice.

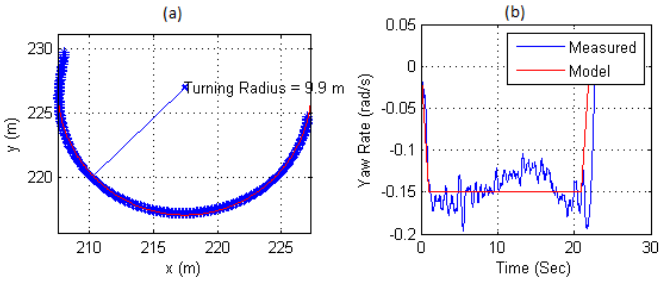

Fig. 14. (a) Turning radius of AUV during the case study (b) Measured yaw rate and modeled yaw rate during the U-turn

the maximum rudder deflection δ_{max} is 0.197 (0.26-0.063) rad. The predicted turning radius is 9.7 m which agrees well with the measured turning radius of 9.9 m. The prediction is accurate as a result from good modeling of the yaw rate as one can see in Fig. 14(b).

VI. Gain-Scheduling Controller Design from Identified Results

The main purpose of system identification is to reconfigure the controller according to the system dynamics. We next present some results on steering control of the STARFISH AUV at different speeds. We would like to demonstrate the ease of controller synthesis after the parameters are obtained and highlight performance improvements after reconfiguration.

Fig. 15 shows the block diagram of the steering control system. We close the loop using a simple proportional (P) controller with a feedforward term. There are two main issues in steering control at different speeds. As the speed changes, the yaw dynamics change too. One solution is to use robust control design methodology which results in selecting a constant gain, K_p that minimizes the norm of the closed-loop transfer function under parametric uncertainty. However, a constant gain robust controller can be very conservative as compared to a gain-scheduled controller that can adapt itself to the change in system dynamics. Another issue in steering control is the steady state error caused by non-zero rudder offset. We handle the issue by feeding forward the term δ_{r_0} to neutralize the offset.

From the block diagram, the closed-loop transfer function from desired yaw ψ_d to yaw output ψ is:

$$\frac{\psi_d(s)}{\psi(s)} = \frac{K_p b_2}{s^2 + a_{22}s + K_p b_2} \tag{67}$$

The closed-loop poles are:

$$p_{1,2} = -\frac{a_{22}}{2} \pm \frac{\sqrt{a_{22}^2 - 4K_p b_2}}{2} \tag{68}$$

TABLE V
Turning Radius for AUV: A case study

a_{22}	b_2	δ_{r_0}	$\dot{\psi}_{max}$ (deg/s)	T_π (s)	R (m)
2.15	-1.62	-0.064	8.47	22.32	9.74

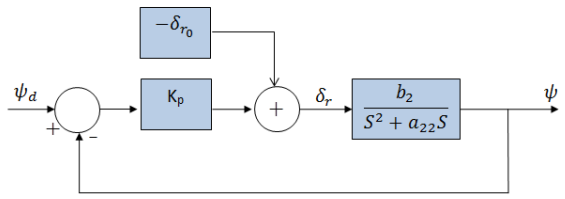

Fig. 15. Block Diagram for Heading Control

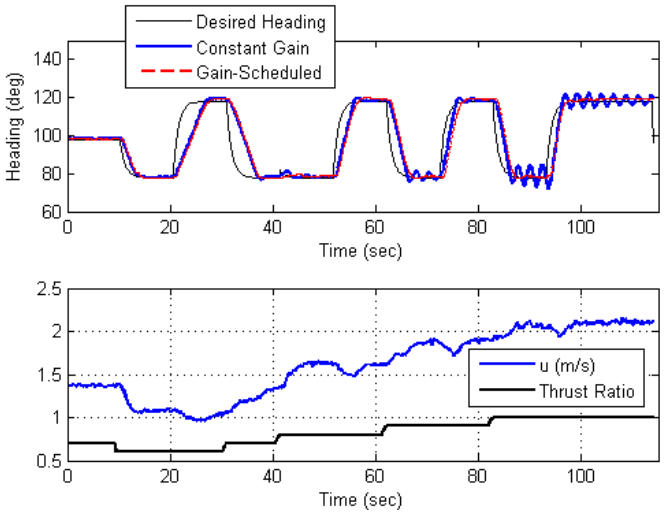

Fig. 16. Experiment results for heading control under constant gain controller and gain-scheduled controller

We select gain K_p such that the closed-loop poles lie in the line of constant damping ratio ζ in the s-plane. For a second order system, the percentage overshoot is only a function of damping ratio. So, we choose ζ to be 0.7071 which equivalent to approximately 5% overshoot. In order to have the poles at constant damping ratio line of 0.7071, we require:

$$-\frac{a_{22}}{2} = \frac{\sqrt{a_{22}^2 - 4K_p b_2}}{2} \Longrightarrow K_p = \frac{a_{22}^2}{2b_2} \tag{69}$$

As shown in section III, a_{22} and b_2 are functions of speed. At different speeds settings, the gain K_p will be adjusted accordingly.

The experimental results obtained using the gain-scheduled controller with feedforward are shown in Fig. 16 with comparison to a constant gain controller. The AUV was first commanded to maintain a constant depth and heading. Then AUV was then commanded to turn ± 20 deg from the current heading while the thrust was increased from 60% to 100%. The constant gain controller performed satisfactory at the lower speed as the constant gain was chosen for this speed setting. In the higher speed region (90% and 100% thrust), the heading response became oscillatory. In contrast, the gain-scheduled controller performed well consistently over the entire speed range.

VII. Conclusion

A common practice of performing system identification each time when the dynamics of the AUV changes is followed by controller redesign based on the updated model. This cycle consumes expensive sea time as well as requires effort from a knowledgeable control engineer to redesign the controller. To address this situation, we developed a technique to enable rapid identification of AUV dynamics online. The technique is based on a state variable filter and the recursive least-square algorithm. We validated the technique by comparing it against an offline method that produces optimal solutions through numerical optimization. Online system identification was performed on both yaw and pitch dynamics at different speeds. We illustrated how yaw identification results can be used to estimate the turning radius of the AUV at different speeds. The accuracy of the estimation was validated in a field experiment. We also show how a gain-scheduled controller could be designed using the identified parameters for steering control. Better control performance was observed as compared to a constant gain controller.

References

[1] M. Caccia and G. Veruggio, "Guidance and control of a reconfigurable unmanned underwater vehicle," *Control Engineering Practice*, vol. 8, no. 1, pp. 21–37, 2000.

[2] P. Ridao, A. Tiano, A. El-Fakdi, M. Carreras, and A. Zirilli, "On the identification of non-linear models of unmanned underwater vehicles," *Control engineering practice*, vol. 12, no. 12, pp. 1483–1499, 2004.

[3] D. Smallwood and L. Whitcomb, "Adaptive identification of dynamically positioned underwater robotic vehicles," *Control Systems Technology, IEEE Transactions on*, vol. 11, no. 4, pp. 505–515, 2003.

[4] M. Rentschler, F. Hover, and C. Chryssostomidis, "System identification of open-loop maneuvers leads to improved auv flight performance," *Oceanic Engineering, IEEE Journal of*, vol. 31, no. 1, pp. 200–208, 2006.

[5] A. Tiano, R. Sutton, A. Lozowicki, and W. Naeem, "Observer kalman filter identification of an autonomous underwater vehicle," *Control engineering practice*, vol. 15, no. 6, pp. 727–739, 2007.

[6] J. Petrich, W. Neu, and D. Stilwell, "Identification of a simplified auv pitch axis model for control design: Theory and experiments," in *OCEANS 2007*. IEEE, 2007, pp. 1–7.

[7] T.-B. Koay, Y.-T. Tan, Y.-H. Eng, R. Gao, M. Chitre, J.-L. Chew, N. Chandhavarkar, R. Khan, T. Taher, and J. Koh, "Starfish – a small team of autonomous robotic fish," *Indian Journal of Geo-Marine Science*, vol. 40, no. 2, pp. 157–167, April 2011.

[8] H. Garnier, M. Gilson, T. Bastogne, and M. Mensler, "The contsid toolbox: A software support for data-based continuous-time modelling," *Identification of Continuous-time Models from Sampled Data*, pp. 249–290, 2008.

[9] J. Kim, K. Kim, H. Choi, W. Seong, and K. Lee, "Depth and heading control for autonomous underwater vehicle using estimated hydrodynamic coefficients," in *OCEANS, 2001. MTS/IEEE Conference and Exhibition*, vol. 1. IEEE, 2001, pp. 429–435.

[10] T. Fossen, "Guidance and control of ocean vehicles," *New York*, 1994.

[11] SNAME, "Nomenclature for treating the motion of a submerged body through a fluid," The Society of Naval Architects and Marine Engineers, Technical and Research Bulletin 1-5, 1950.

[12] B. Jalving, "The ndre-auv flight control system," *Oceanic Engineering, IEEE Journal of*, vol. 19, no. 4, pp. 497–501, 1994.

[13] K. Mahata and H. Garnier, "Direct identification of continuous-time errors-in-variables models," in *Preprints of the 16th World Congress of the International Fedeartion of Automatic Control, July*, 2005, pp. 3–8.

[14] N. S. Nise, *Control systems engineering*, 3rd ed. John Wiley & Sons, 2000.